Talk given at the "VI International Conference on Calorimetry
in High Energy Physics", INFN Frascati (Roma), Italy, June 8-14, 1996.
Published in the Proceedings (Frascati Physics Series)

THE ELECTROMAGNETIC CALORIMETER FOR THE SOLENOIDAL TRACKER AT RHIC.

W.J. Llope for the STAR-EMC Collaboration [1)]
T.W. Bonner Nuclear Laboratory, Rice University, Houston, TX 77005-1892

ABSTRACT

The ElectroMagnetic Calorimeter (EMC) of the Solenoidal Tracker at RHIC (STAR) is a stack of 5 mm lead and 4 mm plastic scintillator layers in the shape of a 4800 tower $\sim$18 X_0 barrel and at least one 540 tower $\sim$25 X_0 endcap. A Shower Maximum Detector (SMD) is placed inside the stack at a depth of $\sim$4.5 X_0. The design of this calorimeter, and the status of the effort to build it, will be described. The construction and performance on the bench of the optical read-out chain will be discussed; particular attention is paid to aspects of the thermal splicing of the plastic optical fibers. A Small Prototype EMC (SPEMC) was constructed and tested in the BNL-AGS B2 line in two runs, resulting in about 1.4 billion events on tape. Five different configurations of the SPEMC were studied systematically for $e^{\pm}$, $h^{\pm}$ (π and p), and $\mu^{\pm}$ at 5-7 momenta in the range from 0.3 to 8 GeV/c and at 12-20 positions on the face of the stack. The configurations differ in the depth segmentation (none, 5/15, or 10/10 in layers) and the angle of incidence (zero or 15°). Selected results from these comprehensive beam tests, both for the stack and the SMDs, will be described.

1 Calorimetry in STAR

The detectors at the Relativistic Heavy-Ion Collider (RHIC) must make sensitive measurements of hadron collisions provided by an extremely flexible machine. RHIC can be tuned to collide two heavy ions of mass A up to ^{197}Au ($\sqrt{s}$=200A GeV), two polarized protons ($\sqrt{s}$=60-500 GeV), or protons and nuclei. This very wide range of entrance channels results in a similarly wide range of final states, each of which may contain fundamental information or signatures of novel phenomena. The first experiment approved at RHIC, called STAR (for the Solenoidal Tracker

At RHIC), is a capable detector for all of the RHIC beams and is presently under construction. [2] This experiment will search for signatures of Quark-Gluon Plasma formation, investigate the behavior of strongly interacting matter at high energy density, and study parton structure functions, Drell-Yan, W and Z production, and other spin-dependent phenomena. Like all other major collider experiments throughout the world, calorimetry is an essential component [3] of STAR.

Proceeding outward from the primary vertex, STAR will consist of a Silicon Vertex Tracker (SVT), a large cylindrical Time Projection Chamber (TPC), a Central Trigger Barrel/Time-of-Flight array (CTB/TOF), an Electromagnetic Calorimeter (EMC), and a room temperature 0.5 T solenoidal magnet. Also included in the design of the apparatus are Forward Time Projection Chambers (FTPCs), Vertex Position Detectors (VPD), as well as forward calorimetry. The Electromagnetic Calorimeter will be a Lead/plastic scintillator sampling calorimeter consisting of a barrel calorimeter (BEMC), barrel Shower Maximum Detectors (BSMDs), two endcap calorimeters (EEMCs), and endcap shower maximum detectors (ESMDs). The BEMC(EEMC) is an $\sim$18(25) radiation length stack of 5 mm thick Lead sheets and 4 mm thick plastic scintillator plates which are read out by 1 mm diameter wavelength-shifting fibers (WSFs). These WSFs are thermally spliced to longer 1 mm diameter clear fibers (CFs), which route the shifted scintillation light out through the magnet coils to externally mounted photo-multiplier tubes (PMTs).

There are 4800(540) projective towers in the BEMC(EEMC). Each tower in the BEMC subtends $(\Delta\eta,\Delta\phi)\sim(0.05, 0.05)$. The initial configuration of the BEMC will likely have the towers that are adjacent in η and ϕ in each module ganged pairwise, resulting in 1200 "instrumented" towers, each subtending $(\Delta\eta,\Delta\phi)\sim(0.1, 0.1)$. Each tower will be segmented in depth to improve the electron/hadron discrimination of the device. The SMDs are wire/strip chambers that are positioned after 5 Lead/scintillator layers ($\sim$4.5 X_0). The pixel size in the SMDs will be on the order of $\sim$1.5cm$\times$1.5cm.

A Small Prototype EMC (SPEMC) was constructed [4] to optimize the construction techniques and study the performance of the stack and several SMD prototypes in test beams appropriate for the RHIC environment. The design of this prototype is based on the design of the BEMC. Results on the optimization of the fiber splices that are part of the stack's optical read-out chain, and the SPEMC/prototype SMD performance in beam will be presented below. Further information on the scintillator wrapping, scintillator/WSF coupling[1], full simulations, and test beam studies have been presented [3, 5, 6] in the preceding conferences in

[1] We note that a different approach for the scintillator/WSF coupling (an "α-groove") will be studied in prototype BEMC and EEMC modules that are presently under construction.

this series.

2 Optical Fiber Splicing

Due to space limitations and the relatively high cost of magnetic field-insensitive PMTs, the scintillation light is to be shifted and carried outside of the magnet coils to externally mounted PMTs. Round 1 mm diameter plastic optical fibers will be circuitously routed over a path that's $\sim$3 m long, which is large compared to the typical attenuation length of WSFs. We have therefore adopted a design similar to that used in the CDF calorimeters [7], which involves the thermal splicing of 20-35 cm long WSFs to $\lesssim$3 m long CFs. If this method is to work, one must simultaneously maximize the optical transmission efficiency at each splice, minimize the splice-to-splice variation in this transmission, and maximize the mechanical strength of the splice joint. The fibers used in this study and in the SPEMC are Bicron BCF-91A.

The thermal splicing was done using an automated device [8] developed by the Michigan State University - High Energy Physics group for use in the construction of CDF calorimeters. [7] As the optical fibers for the STAR-EMC differ from those used in the CDF calorimeters, it is important to re-explore the parameter space of this fiber splicer for the present application. The mechanical strength and optical transmission efficiency of the splices can depend strongly (and often inversely) on the various splicer settings.

The operation of the MSU-HEP fiber splicer is highly automated, which results in very consistent splices. Four time intervals and two pressures are adjustable, but in general the most important parameter is the heating time. This is the time interval over which a modified projector lamp melts the two fibers where they meet. The fibers are held inside a short section of preshrunk FEP tubing (the "jacket"), which is enclosed by a pair of precision milled glass half tubes.

A side view of a typical splice is shown in Figure 1. The splices obtained from this device look similar to those obtained from other optical fiber splicers. [9] The jacket increases the splice width, but it also adds a considerable amount of strain relief to the joint.

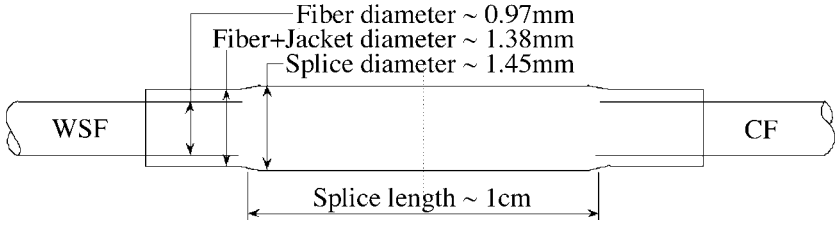

Figure 1: A dimensioned side view of the typical splice used in the SPEMC.

The mechanical strength of the splices were studied versus the heating time and the other splicer parameters in two different ways. The strength longitudinally was studied using a machine provided by the MSU-HEP group which held the fiber on both sides of the splice and pulled by increasing amounts. Undeformed splices typically had longitudinal strengths within ∼20% of that for lengths of the same fiber without a splice, supporting more than 10 lbs. of force along the fiber. The "transverse" strength is a somewhat more critical attribute, as the fibers may be bent over radii of curvature ≳3.0 cm near the splice. This bending strength depends more strongly on the splicer parameters than the longitudinal strength. It was evaluated by bending spliced fibers in a circle at the splice and measuring the radius of this circle that results in the breaking of the splice joint.

The strongest splices have minimal break radii, while Liouville's theorem [10] demands light losses of an amount increasing with the splice length[2]. The best heating time thus results in a minimal break radius and a minimal splice length. The break radius and the splice length are shown versus the heating time in Figure 2. The splice length increases linearly with the heating time in the range from 5 to 15 s. As the heating time is increased, however, the break radius of the splice decreases, *i.e.* the splices become mechanically stronger. For heating times in the range from 10 to ∼14 seconds, the splice joints do not break for radii of curvature that are ≳0.5 cm. Here the splice joint is stronger than the fiber itself, as for radii ≲1.5 cm, the fibers themselves more often break where they enter the jacket.

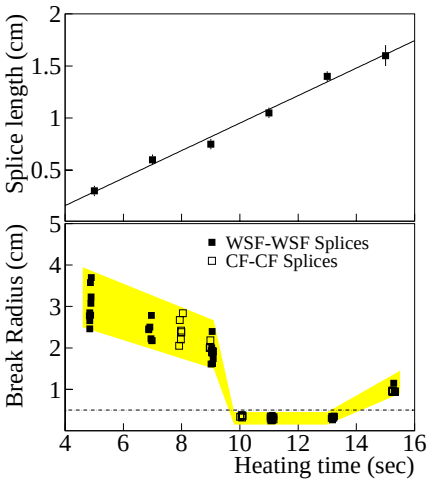

Figure 2: The splice length (upper frame) and the break radius (lower frame) versus the heating time.

We therefore set the heating time at 11 s for the SPEMC fibers. This safely results in the shortest possible splice lengths for essentially unbreakable splices. The

[2]Increasing the splice diameter relative to the fibers also increases light loss at the splice according to this theorem, but the splice diameter is held constant to ∼1 mil by the splicer.

focus was then directed onto maximizing the optical transmission efficiency of the splices over the more limited range of splicer parameters leading to unbreakable splices. However, unlike the mechanical properties, the optical transmission efficiency can be significantly affected by the quality of the fiber preparation before the splicing.

A linear scanner including a collimated UV light source and reference measurements was used to measure the shifted light transmission as a function of the position along unspliced WSF fibers and spliced WSF+WSF fibers. These measurements were used to extract the optical transmission efficiency for shifted light across each splice, which was tabulated versus different splicer settings following different methods used to prepare the fibers before splicing.

Besides the optical transmission from the linear scanner, there are two splice properties that can be evaluated visually with a hand-held UV light source. The first is splice deformation (either along the splice or azimuthally), which results from the occasional uneven heating of the joint producing a mechanically weak and optically inefficient splice. The second is by far the most important contributor of optical transmission inefficiencies. If the cladding on one or both fibers is damaged during the cutting of these fibers, a break in the cladding exists where the (spliced) fibers meet, which allows a significant amount of light to escape. The splices were therefore classified into three categories ("gold", "silver", and "bronze") on the basis of the visual inspection with a hand-held UV source. The best splices ("gold") were undeformed and showed no cladding breaks. The next best class of splices ("silver") were either slightly deformed, or showed small cladding breaks (typically less than $\sim$1/3 of the circumference of the splice). The apparently worst splices ("bronze") were either very deformed or had large cladding breaks, or both.

The typical results from the linear scanning is shown in Figure 3. The left frame shows the dependence of the shifted light output on the linear distance between the collimated UV source and a PMT which are "connected" by a straight unspliced WSF fiber. The core attenuation length was consistently measured to be 1.8 m. Exponential fits to the transmission curves for spliced fibers were employed with fixed attenuation lengths to extract the transmission efficiency of shifted light across each WSF to WSF splice. Examples of these fits for typical gold, silver, and bronze splices are shown in the right frame of Figure 3.

The attributes of the splices evaluated by the visual inspection under a UV light source (*i.e.* splice deformation and/or cladding breaks) were strongly correlated with the transmission efficiencies measured by the linear scanner. This is because the splice dimensions are fixed at the constant values appropriate for the final set of splicer parameters. Thus, Liouville's theorem contributes much less to the splice-to-

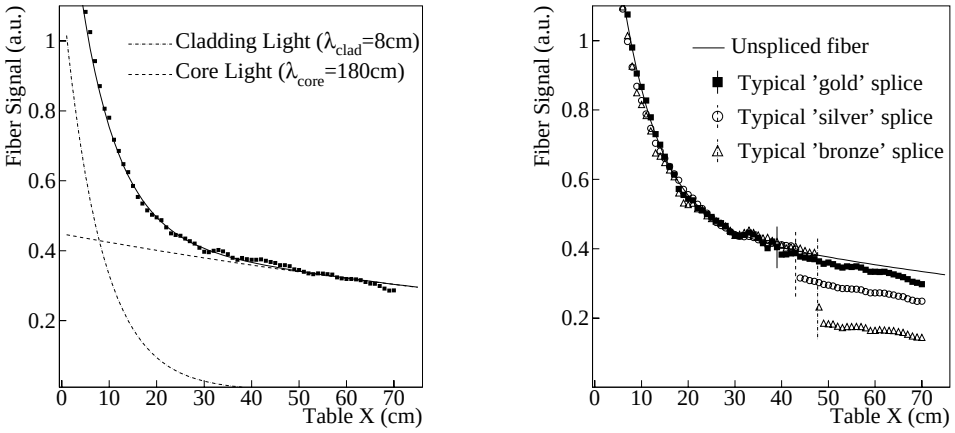

Figure 3: The light output at the end of unspliced (left frame) and spliced fibers of various qualities (right frame).

splice variations in the transmission as compared to sloppy fiber preparation, which results in visually apparent cladding breaks, and rarely, splice deformation. The optical efficiencies obtained were (92±4)%, (80±10)%, and (65±20)% for the gold, silver, and bronze splices, respectively. The optical efficiency of our gold splices is consistent [8] with that obtained by the CDF group for their best splices, although our fibers have a larger diameter and different manufacturer, and our set of splicer parameters are different.

The 240 spliced fibers needed for the SPEMC were then produced. As the fiber preparation is by far the most important aspect of the production of consistently high quality splices, considerable care was taken to cut the WSFs and CFs using a jig that minimized damage to the fiber cladding. During the final production, approximately 14/15 of the splices were visually classified as golden. Loading the fibers in the preshrunk jacket, inserting these into the splicer, and running the splicer takes about 90 seconds per splice. Cladding breaks are essentially eliminated altogether by polishing the two ends to be spliced using another automated device (also developed for the construction of the CDF calorimeters). This polishing takes about 60 s/splice, but it leads to gold splices essentially every time.

The SPEMC was then assembled using a scintillator wrapping and scintillator/WSF coupling technique involving Tyvek paper and Aluminized mylar that results in an average of 1.75 photoelectrons [5] per minimum ionizing particle for WSFs(CFs) that were 18(200) cm long. In the SPEMC, the scintillator was Kurrary SCSN38 and the Lead was unclad and unalloyed. The scintillators were arranged in six towers, four(two) of which were the same size as the BEMC towers at $\eta \sim 0(1)$. An aluminum box was placed in the stack after 5 lead/scintillator layers ($\sim$4.5 X_0) to allow the insertion of different prototype SMDs. Selected results from the in-beam tests of the SPEMC and the prototypical SMDs are described in the next section.

3 SPEMC and SMD Performance

The SPEMC was studied in beam at the Brookhaven AGS B2 line in two runs in May 1994 and July 1995. Five different configurations of the SPEMC were studied systematically for $e^{\pm}$, $h^{\pm}$ (π and p), and $\mu^{\pm}$ at 5-7 momenta in the range from 0.3 to 8 GeV/c and at 12-20 positions on the face of the stack. The configurations differ in the depth segmentation (none, 5/15, or 10/10 in layers) and the angle of incidence (zero or 15°). Three different prototype SMDs were inserted into the SPEMC stack to study their performance as well. A high speed transputer data acquisition system was used, which allowed event rates to tape approaching 15 kHz, and resulted in over 1.4 billion events on tape in total.

The SPEMC energy resolution and linearity for electrons is shown in Figure 4. This resolution is consistent with that from similarly designed EMCs in other experiments, and better than the $\sim 20\%/\sqrt{E}$ design goal for the STAR-EMC. The SPEMC is linear to better than 1% for electron energies below ~6 GeV/c after the correction [11] for the electron energy loss in the beam-line.

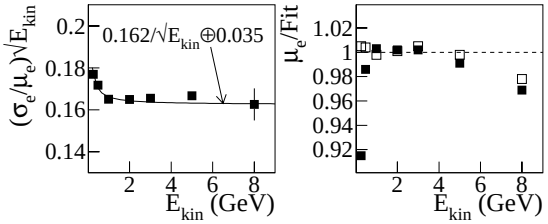

Figure 4: The energy resolution (left frame) and the linearity (right frame) of the total signal from the SPEMC stack for electrons. The linearity is shown before (solid points) and after (open points) the correction for the electron energy loss in the beam-line.

Of the three SMDs that were studied in beam, one was a scintillator/fiber/PMT design ("SciFi") and the other two were wire/strip chambers. The SciFi SMD consists of two layers, each of which consists of a 2 mm thick Lead plate and 5mm thick by 1.4 cm wide scintillator strips. It is just under one X_0 in thickness, which is considerably thicker in radiation lengths than either of the prototype wire/strip chamber SMDs. This will be apparent in the results shown below.

Due to significant differences in the cost, wire/strip chambers will be the SMD technology used in the STAR-EMC. The design of the two different wire/strip SMD prototypes that were studied in the SPEMC is similar to that for the SMDs in CDF. The following will concentrate on the results obtained from one of these chambers, called "ASMD"; the data from the other SMD is being analyzed independently. The wire(strip) pitch in the ASMD was (0.725)1.56 cm, and the wires were ganged in two per read-out channel. The gas was 5% CO_2 and 95% Argon, while the

Voltage was ∼1400 V. There were transresistance amplifiers on the chamber itself, all of which where within ∼2 cm of the wires or strips.

The ASMD gas volume was inside an aluminum foil EM shield which was isolated from both the ASMD ground and the SPEMC ground. This ground was connected to the cable shield. On the basis of SPICE simulations (see below), the twisted-pair signal cables were shielded with aluminum foil and an outside insulator. On the other end of these ∼20 meter signal cables, there were MAX436 differential receiver chips before the ADCs. The cable shield was connected to ground only at the receiver end.

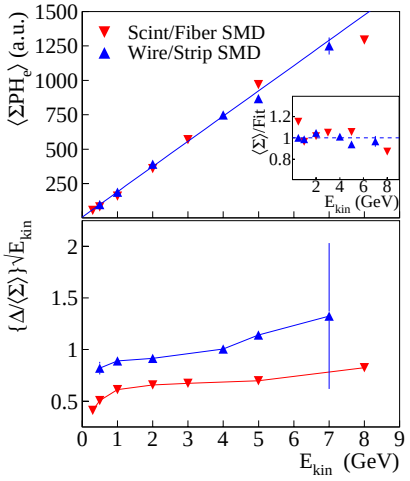

Figure 5: The SMD summed pulse height response (upper frame) and pulse height resolution (lower frame) versus the energy of electrons incident on the SPEMC for the SciFi SMD (down triangles) and the ASMD (up triangles). The inset depicts the linearity of the SMD total pulse heights without any constraint on the depth of the shower maximum (see text).

The average values of the total pulse height distributions from the SciFi SMD and the ASMD are shown versus the electron energy in Figure 5. Without any constraint on the depth of the shower maximum via a cut on the front/back energy sharing in the depth segmented SPEMC, the average total pulse heights from both SMDs is linear to ∼15%. Employing such a gate to select showers with maxima near the SMD layer, the SMD signal linearity can be improved by a factor of two. The lower frames of Figure 5 depict the energy weighted SMD pulse height resolution, $\Delta\sqrt{E}/\Sigma$, where Σ and Δ are the average and standard deviation of the pulse height distribution for electrons of an energy E. The ratio Δ/Σ for the SciFi SMD thus behaves like $\sim 0.6/\sqrt{E}$, while the ASMD resolution goes like $\sim 1/\sqrt{E}$. The considerably better pulse height resolution obtained from the SciFi SMD is the natural result of its much larger thickness in radiation lengths.

Like the optical fibers for the stack, the signal cables for the (wire/strip

chamber) SMDs in STAR are routed out radially through the magnet coils. The STAR magnet coils could potentially have a voltage ripple of a few hundred Volts, but this could be reduced to ~20 V with some filtering of the magnet power. A test was therefore performed to evaluate the performance of the SMD with and without the presence of a (simulated) capacitively coupled noise signal from a magnet coil.

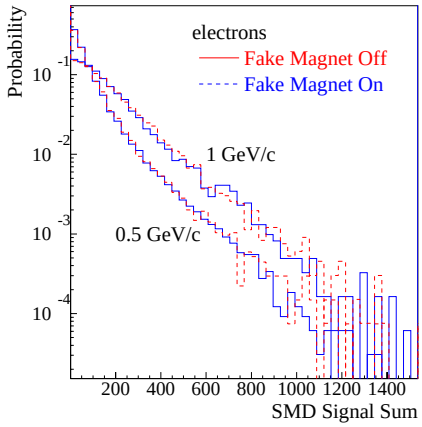

Figure 6: The total pulse height distributions obtained from a prototype wire/strip SMD in the SPEMC for 0.5 GeV/c and 1.0 GeV/c electrons, as labelled, with the simulated magnet noise signal off (solid lines) and on (dashed lines).

To simulate the magnet noise, a 20 V square wave (1 kHz rate, 1 μs rise time) was added though ~500 pF to the ASMD cable shield. The summed pulse height distributions obtained from the ASMD when low energy electrons are directed at the SPEMC are shown in Figure 6. The solid and dashed histograms show what is obtained with the fake magnet off and on, respectively. No modification of the summed pulse heights, or the signals from individual ASMD channels (not shown), is apparent. The shielding of the ASMD and its cables that was described above thus provides the necessary protection from ~20 V magnet noise that is coupled through ~500 pF.

4 Electron/hadron Discrimination

The direct identification of electrons with momenta above a few GeV/c in STAR is possible only with the information provided by the EMC. As the SPEMC and all three prototype SMDs worked well in the test beam, it is relevant to explore the electron/hadron discrimination that is possible using a variety of cuts on both stack and SMD observables.

For SMD-equipped EMCs that are segmented into two depth sections, the six observables shown in Figure 7 support cuts that provide e/h discrimination for hits of known momentum.[3] The stack observables are the total energy ("SPEMC

[3]In the test beam, this was controlled via the beam line magnets, while in STAR, track momenta

ΣPH"), the front, F, to back, B, energy sharing quantified by $Z=(B-F)/(B+F)$ ("Cal-Z"), and the ratio of the struck tower energy to the total ("isolation"). The SMD observables are the total pulse height ("SMD ΣPH"), the pulse-height weighted shower width in both the X and Y directions in centimeters ("SMD $\Delta X \oplus \Delta Y$"), and the difference between the expected location of the shower centroid and the measured shower centroid ("$\vec{X}_{smd}-\vec{X}_{pred}$").

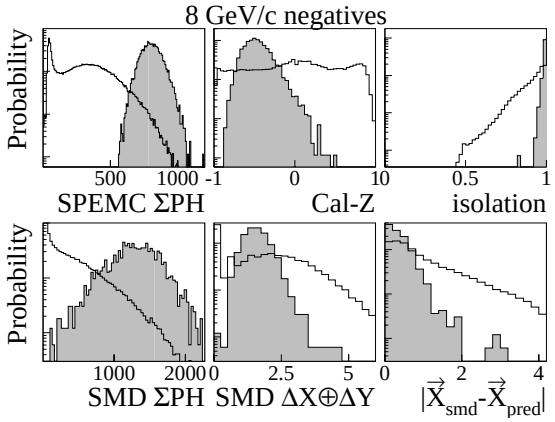

Figure 7: Three stack observables (upper frames) and three SMD observables (lower frames) that support cuts leading to e/h discrimination, shown for 8.0 GeV/c electrons (shaded histograms) and hadrons (open histograms).

The geometry of the actual STAR-EMC is somewhat different from the SPEMC geometry, while the test beam data cannot include the tower and SMD channel occupancy expected in RHIC events. We have thus concentrated only on simple and approximately located cuts to get a feel for the general trends.

At momenta below ∼1.5 GeV/c, the most effective cuts are the E/p cut and the front/back energy cut. For larger momenta, the front/back energy cut becomes less effective, while the E/p cut and all of the SMD-based cuts become more effective. Using reasonable but unoptimized cuts on these two combinations of observables, the discrimination is roughly 6:1 at electron efficiency of ∼80% for momenta below ∼1 GeV/c. In this range of momenta, however, other detectors in STAR, primarily the STAR TOF, also provide e/h discrimination capabilities. At momenta above 2 GeV/c, the discrimination is $\gtrsim$100:1 and the electron efficiency is between 60 and 80%.

5 Outlook

This contribution described results obtained during the construction and in-beam tests of a small calorimeter composed of BEMC towers and several prototype SMDs.

are provided by the TPC and the SVT.

At present, a mechanical prototype of a BEMC module is being studied to optimize the module construction techniques and fiber routing. A fully functional module of the EEMC is also under construction. The development of prototype electronic components and the detailed simulation of the EMC as a part of STAR continues as we prepare to be ready for the first day of RHIC beams in the summer of 1999.

6 Acknowledgements

This work was supported by the U.S. Department of Energy under the Grant No. DE-FG03-93ER40772. We are grateful to R. Richards, J. Huston, D. Shooltz, J. Mansour, and B. Tannenbaum (MSU-HEP group) for helpful discussions and the use of their fiber splicer, polisher, and linear scanner.

References

1. Argonne National Laboratory, Brookhaven National Laboratory, IHEP - Protvino, JINR - Dubna, Lawrence Berkeley Laboratory, Michigan State University, Penn State University, Rice University, Wayne State University, University of California - Los Angeles, and University of New Mexico.

2. http://rsgi01.rhic.bnl.gov/star/starlib/doc/www/star.html

3. G.D. Westfall, published in the Proceedings of the V International Conference on Calorimetry in High Energy Physics, Brookhaven, N.Y. (1994).

4. http://bonner-mac8.rice.edu/~WJLlope/

5. D.G. Underwood, published in the Proceedings from the IV International Conference on Calorimetry in High Energy Physics, La Biodola, Elba (1993).

6. D.G. Underwood, published in the Proceedings of the V International Conference on Calorimetry in High Energy Physics, Brookhaven, N.Y. (1994).

7. http://www-cdf.fnal.gov/

8. R. Richards, private communication; B. Tannenbaum, Masters Thesis, Michigan State University, unpublished (1994); J.P. Mansour *et al.*, /CDF/DOC/PLUG_UPGR/PUBLIC/2562.

9. G. Apollinari *et al.*, Nucl. Inst. and Methods **A311**, 520 (1992).

10. K.G. Steffen, *High Energy Beam Optics*, pgs. 161-172 (Interscience Publishers, New York, N.Y.).

11. A. Patwa *et al.*, PHENIX Technical Note 181 (1995).